

# Trifocal Tensor and Relative Pose Estimation with Known Vertical Direction

Tao Li<sup>1</sup>, Zhenbao Yu<sup>2,3</sup>, Banglei Guan<sup>2\*</sup>, Jianli Han<sup>1</sup>, Weimin Lv<sup>1</sup> and Friedrich Fraundorfer<sup>4</sup>

**Abstract**—This work presents two novel solvers for estimating the relative poses among views with known vertical directions. The vertical directions of camera views can be easily obtained using inertial measurement units (IMUs) which have been widely used in autonomous vehicles, mobile phones, and unmanned aerial vehicles (UAVs). Given the known vertical directions, our algorithms only need to solve for two rotation angles and two translation vectors. In this paper, a linear closed-form solution has been described, requiring only four point correspondences in three views. We also propose a minimal solution with three point correspondences using the latest Gröbner basis solver. Since the proposed methods require fewer point correspondences, they can be efficiently applied within the RANSAC framework for outliers removal and pose estimation in visual odometry. The proposed method has been tested on both synthetic data and real-world scenes from KITTI. The experimental results show that the accuracy of the estimated poses is superior to other alternative methods.

**Index Terms**—Vision-Based Navigation, Visual-Inertial SLAM, Sensor Fusion.

## I. INTRODUCTION

WITH the rapid development of autonomous navigation, autonomous driving, and augmented reality, the combination of camera and IMU is becoming increasingly popular. The camera offers the benefits of non-contact operation, high precision, miniaturization, cost-effectiveness, and rich information. Meanwhile, IMU can deliver precise short-term position, velocity, acceleration, and angle data solely through internal sensors without external assistance. So there is a high degree of complementarity of the advantages between cameras and IMUs. The combination of cameras and IMUs has become an indispensable equipment for moving platforms, so the fusion technology of cameras and IMUs has received

This paper was recommended for publication by Editor Pascal Vasseur upon evaluation of the Associate Editor and Reviewers' comments. This work was supported in part by the Hunan Provincial Natural Science Foundation for Excellent Young Scholars under Grant 2023JJ20045, and the National Natural Science Foundation of China under Grant 12372189. Corresponding author: Banglei Guan.

<sup>1</sup>Tao Li, Jianli Han, and Weimin Lv are with the College of Aerospace Science and Engineering, Naval Aeronautical University Yantai 264000, China litao0931@alumni.nudt.edu.cn, jianlihan1585@163.com, 2016150315@jou.edu.cn

<sup>2,3</sup>Zhenbao Yu is with the College of Aerospace Science and Engineering, National University of Defense Technology, Changsha 410000, China and the Global Navigation Satellite System Research Center, Wuhan University, Wuhan 430000, China zhenbaoyu@whu.edu.cn

<sup>2</sup>Banglei Guan is with the College of Aerospace Science and Engineering, National University of Defense Technology, Changsha 410000, China guanbanglei12@nudt.edu.cn

<sup>4</sup>Friedrich Fraundorfer is with the Institute of Computer Graphics and Vision, Graz University of Technology, Graz, Austria friedrich.fraundorfer@tugraz.at

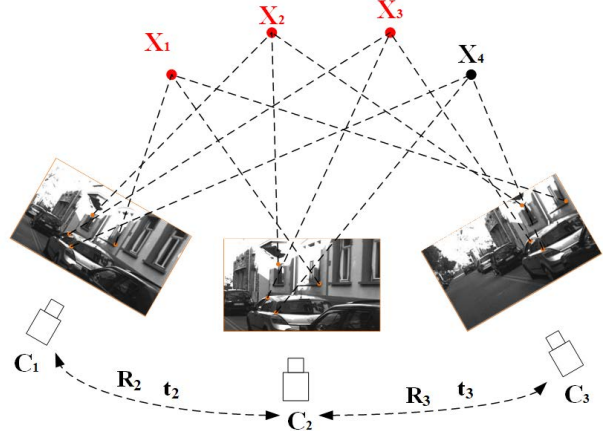


Fig. 1. Trifocal tensor using 4 point correspondences or 3 point correspondences in three views.

more and more attention [1]. In particular, Carlos Campos et al. have applied vision and IMU fusion technology to the ORB-SLAM3 [2] algorithm and its accuracy has improved dramatically compared to ORB-SLAM2 [3].

Estimating the relative pose is the most critical step in computer vision fields, including simultaneous localization and mapping (SLAM) and structure from motion (SfM) [4]. The relative pose estimation of two views is already very mature, but there are still many difficulties and challenges in the pose estimation of the 3-view problem, such as the typical 3v4p (3-view 4-point) perspective pose problem [5], see Fig. 1. But overall, compared with the 2-view pose estimation represented by epipolar constraints, the 3-view pose estimation has the advantage of requiring fewer matching features and undergoing less degeneration [6], for its constraints are tighter. Since the solution of the 3-view problem is more complex and time-consuming, it should not be regarded as a replacement or a competitor for 2-view pose estimation, but rather as a fallback option when the 2-view pose estimation fails [7].

In practice, there will be mismatched features, so combining the pose estimation algorithms with robust estimation frameworks is necessary. The most commonly used robust framework is the random Sample Consensus (RANSAC) [8], and its iteration numbers are closely related to the minimum sample size required. In general, the number of iterations increases exponentially as the number of matching features required by the algorithm increases. Therefore, it is of great significance to minimize the number of matches needed by the algorithm, because it can effectively boost the efficiency and robustness of pose estimation.

The minimum solution plays an important role in addressing

geometric vision problems. In the classic 2-view pose estimation problems, the rotation matrix  $\mathbf{R}$ , and the translation vector  $\mathbf{t}$  each consists of 3 unknowns, so 5 unknowns still need to be solved without considering scale ambiguity. The most typical method is Nister's 5-point method [9], which applies Gauss-Jordan elimination method to reduce the polynomial equations. For the 3-view pose estimation problem, theoretically, 4 point correspondences or 6 line correspondences are enough to solve the camera pose for three views [10]. However, these solvers may produce more spurious solutions due to nonlinear constraints, such as up to 600 solutions with the 6-line method [11]. Ding proposed to solve the 3-view problem using the HC (homotopy continuation) solver, which needs GPU implementations for parallel calculations, so it is also called GPU-HC solver [6]. Fabbri et al. also proposed two minimum solutions based on the HC solver [12]. Inspired by [13], the main contributions of this paper can be summarized as follows.

- By fusing IMU information into the 3-view problem, the linear closed-form solution with 4 point correspondences can be derived. Compared with the latest 4-point method, our method can operate in real-time on CPU, which is more efficient, simple, and practical.
- We propose a new minimal solver using only 3 point correspondences, which uses fewer point correspondences than other 3-view problem solvers. The minimum problem can be converted into two polynomials with two unknowns about rotation angles among three views. The maximum polynomial degree is 12, and the minimal solver is found with the automatic Gröbner basis solver.
- In extensive synthetic and real experiments, we have proved that the proposed methods can achieve higher accuracy than the traditional 3-view problem linear solver, and even higher than the accuracy of the classic 2-view problem solvers.

The rest of this paper is arranged as follows. In Section II, the related studies are reviewed. In Section III, the 3pt-Our-3view and 4pt-Our-3view methods are proposed, and their detailed principles are deduced. In Section IV, the performance of the proposed methods is tested using both synthetic and real-world datasets. Finally, we present the conclusions in Section V.

## II. RELATED WORK

Since 3-view problem solving is still a hard problem [5], as far as we know, there are few publicly available solvers for the 3-view problem. The problem has 12 degrees of freedom, where the rotation matrix  $\mathbf{R}$  and the translation vector  $\mathbf{t}$  each consists of 6 unknowns.

**3-view point-based problems:** For the 3-view point-based problem, Heyden et al. introduced the concept of reduced fundamental tensor and proposed that solving the trifocal relative pose at least needs 6 points [14]. Based on algebraic constraints of the correlation slices, Ressl et al. proposed the minimal parameterization of the trifocal tensor [15]. Nordberg et al. introduced three  $3 \times 3$  orthogonal matrices which can transform the original trifocal tensors into a sparse form with only 10 non-zero parameters up-to-scale [16]. Faugeras et al.

presented a set of 12 algebraic equations that serve as adequate constraints for characterizing a trifocal tensor [17]. Ponce et al. proposed 6 homogeneous constraints that can be obtained through a projective transformation of the space, and explored a new approach to characterize the 3-view model [18]. The most relevant paper to our research is [6], Ding et al. solved minimal problems with 4 point correspondences in three views and illustrated the effective use of GPU implementations for the Homotopy Continuation solver. The solver needs to train a model to predict a starting solution for the Homotopy Continuation method in order to obtain a satisfactory solution [19]. Xu et al. proposed an accurate and real-time point-line based pose estimator that fully exploits the correlation constraints of points and lines, making it able to handle both general and degenerate cases [20].

**Polynomials solvers:** It is well known that pose estimation problems can be converted into polynomial solving. Kukelova et al. first presented the automatic Gröbner basis solver, which has been widely used for minimal problems [21]. However, the Gröbner solver is unstable and difficult to solve large-scale problems, but now with the deepening of related research, the stability and speed of Gröbner basis methods have been further improved [22]. Based on [21], Larsson et al. proposed a more efficient solver that can exploit intrinsic relations of the input polynomials [23]. Li et al. proposed the GAPS solver, and the efficiency, usability, and flexibility of the solver have all been improved [24]. Bhayani et al. studied an alternative algebraic method that can convert resultant constraints to eigenvalue problems [25]. Martyushev et al. proposed the latest Gröbner basis solver for Laurent polynomial equations, which can check whether the equations meet the requirements for building the elimination template [26]. Ding et al. proposed some new insights into minimal solvers based on elimination theory, which helps generate more efficient solvers [27] [28]. In addition, the HC solver is also an effective numerical solver for polynomials solving [29]. Recent studies have shown that trifocal tensor can be effectively resolved by GPU-HC solver, for it can accelerate the speed in orders of magnitude, but they are still limited by the computer hardware level [30]. Since the HC solver needs a starting solution and higher hardware configuration, we still use the latest Gröbner basis solver in this paper.

## III. POSE ESTIMATION

### A. Trifocal Tensors

Based on the camera projection model described in [10], the camera's projection matrix can be represented as  $\mathbf{P} = \mathbf{K}[\mathbf{R} \mid -\mathbf{R}\tilde{\mathbf{C}}]$ , where  $\tilde{\mathbf{C}}$  is the world coordinate of the camera's center. Assuming  $\mathbf{X}$  is a spatial 3D point, its image coordinate  $\mathbf{x}$  can be represented as  $\mathbf{x} = \mathbf{P}\mathbf{X}$ . When the camera calibration matrix  $\mathbf{K}$  is known, we can obtain its normalized image coordinate  $\hat{\mathbf{x}} = \mathbf{K}^{-1}\mathbf{x}$ . This implies that  $\hat{\mathbf{x}}$  is the corresponding image point of  $\mathbf{X}$  under the camera with the calibration matrix  $\mathbf{K} = \mathbf{I}$ , where  $\mathbf{I}$  denotes the identity matrix. In order to remove the influence of camera calibration matrices, we define  $\hat{\mathbf{P}} = \mathbf{K}^{-1}\mathbf{P} = [\mathbf{R} \mid -\mathbf{R}\tilde{\mathbf{C}}]$  as the normalized projection matrix. In the following paragraphs, all

the camera calibration matrices are assumed to be intrinsically calibrated, and all projection matrices and image coordinates are normalized projection matrices and normalized image coordinates.

In the three views, the projection matrix for each camera can be represented as:

$$\mathbf{P}_k = \begin{bmatrix} 1 & 0 & 0 & 0 \\ 0 & 1 & 0 & 0 \\ 0 & 0 & 1 & 0 \end{bmatrix} \begin{bmatrix} \mathbf{R}_k & -\mathbf{R}_k \mathbf{t}_k \\ \mathbf{0} & 1 \end{bmatrix}, \quad (1)$$

where  $k = 1, 2, 3$ ,  $\mathbf{P}_k$  is the projection matrix of the  $k$ -th camera. Assuming that the first view is at the origin of the world coordinate system, i.e.  $\mathbf{R}_1 = \mathbf{I}_{3 \times 3}$ ,  $\mathbf{t}_1 = [0, 0, 0]^T$ ,  $\mathbf{R}_k$  and  $\mathbf{t}_k$  denote the rotation matrix and translation vector between the  $k$ -th view and the first view, respectively.

In order to facilitate the derivation of trifocal tensors, the projection matrices can be expressed as  $\mathbf{P}_1 = [\mathbf{I} | \mathbf{0}]$ ,  $\mathbf{P}_2 = [\mathbf{A} | \mathbf{a}_4]$  and  $\mathbf{P}_3 = [\mathbf{B} | \mathbf{b}_4]$ , respectively.  $\mathbf{A}$  and  $\mathbf{B}$  are  $3 \times 3$  matrices, and  $\mathbf{a}_i$  and  $\mathbf{b}_i$  represent  $i$ -th columns of corresponding projection matrices. It is worth noting that  $\mathbf{a}_4$  and  $\mathbf{b}_4$  are the epipoles generated by the first camera in the second and third views respectively, i.e.  $\mathbf{e}'$  and  $\mathbf{e}''$ . Then, the trifocal tensors of the three views can be expressed as:

$$\mathbf{T}_i = \mathbf{a}_i \mathbf{b}_4^T - \mathbf{a}_4 \mathbf{b}_i^T, \quad i = 1, 2, 3. \quad (2)$$

In the common case, the rotation transformation between views belongs to the Euclidean transformation, which can be characterized by yaw, pitch, and roll angles. Using the measurement information of IMUs, the pitch and roll angles of each view can be obtained. Then, the camera's y-axis can be aligned to the direction of gravity, i.e., the y-axis is perpendicular to the ground plane, see Fig. 2.

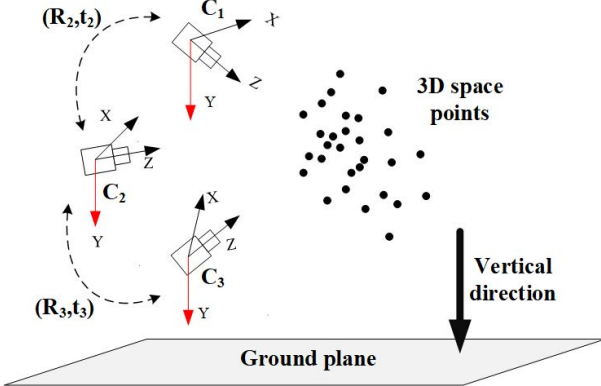


Fig. 2. Camera alignment with known vertical direction.

Assuming  $\tilde{\mathbf{x}}^k$  represents the image point,  $\mathbf{R}_{\text{imu}}$  denotes the alignment matrix of  $k$ -th view. After alignment, its aligned image point  $\mathbf{x}^k$  can be represented as:

$$\mathbf{x}^k = \mathbf{R}_{\text{imu}} \tilde{\mathbf{x}}^k. \quad (3)$$

Similarly, in the following paragraphs, all the image points are pre-aligned, i.e., aligned image points. Then, the rotation transformation  $\mathbf{R}_k$  is only related to the yaw angle, the pose transformation after alignment can be expressed as:

$$\mathbf{R}_k = \begin{bmatrix} C_y^k & 0 & S_y^k \\ 0 & 1 & 0 \\ -S_y^k & 0 & C_y^k \end{bmatrix}, \mathbf{t}_k = \begin{bmatrix} t_x^k \\ t_y^k \\ t_z^k \end{bmatrix}, \quad (4)$$

where  $\theta_k$  represents the yaw angle of  $k$ -th view and  $C_y^k = \cos(\theta_k)$ ,  $S_y^k = \sin(\theta_k)$ .

Conversely, the original relative pose transformation  $\tilde{\mathbf{R}}_k$  and  $\tilde{\mathbf{t}}_k$  can be recovered from the following equations:

$$\begin{aligned} \tilde{\mathbf{R}}_k &= (\mathbf{R}_{\text{imu}})^T \mathbf{R}_k \mathbf{R}'_{\text{imu}} \\ \tilde{\mathbf{t}}_k &= (\mathbf{R}_{\text{imu}})^T \mathbf{t}_k \end{aligned}, \quad (5)$$

where  $\mathbf{R}'_{\text{imu}}$  represents the alignment matrix of the first view,  $\mathbf{R}_{\text{imu}}$  represents the alignment matrix of  $k$ -th view.

### B. The 4-point Case

Substituting (4) into (1), the projection matrix can be expressed as:

$$\mathbf{P}_k = \begin{bmatrix} C_y^k & 0 & S_y^k & -C_y^k t_x^k - S_y^k t_z^k \\ 0 & 1 & 0 & -t_y^k \\ -S_y^k & 0 & C_y^k & S_y^k t_x^k - C_y^k t_z^k \end{bmatrix}. \quad (6)$$

Then, substituting  $\mathbf{a}_i$  and  $\mathbf{b}_i$  from columns of  $\mathbf{P}_k$  into (2), we can deduce the trifocal tensors as follows:

$$\mathbf{T}_1 = \begin{bmatrix} Q_1 & Q_2 & Q_3 \\ Q_4 & 0 & Q_5 \\ Q_6 & Q_7 & Q_8 \end{bmatrix}, \quad (7)$$

$$\mathbf{T}_2 = \begin{bmatrix} 0 & Q_9 & 0 \\ Q_{10} & Q_{11} & Q_{12} \\ 0 & Q_{13} & 0 \end{bmatrix}, \quad (8)$$

$$\mathbf{T}_3 = \begin{bmatrix} Q_{14} & -Q_7 & Q_{15} \\ -Q_5 & 0 & Q_4 \\ Q_{16} & Q_2 & Q_{17} \end{bmatrix}, \quad (9)$$

where

$$\begin{cases} Q_1 = C_y^3 Q_9 + C_y^2 Q_{10}, & Q_2 = -C_y^2 t_y^3, \\ Q_3 = C_y^2 Q_{12} - S_y^3 Q_9, & Q_4 = C_y^3 t_y^2, \\ Q_5 = -S_y^3 t_y^2, & Q_6 = -S_y^2 Q_{10} + C_y^3 Q_{13}, \\ Q_7 = S_y^2 t_y^3, & Q_8 = -S_y^2 Q_{12} - S_y^3 Q_{13}, \\ Q_9 = C_y^2 t_x^2 + S_y^2 t_z^2, & Q_{10} = -C_y^3 t_x^3 - S_y^3 t_z^3, \\ Q_{11} = t_y^2 - t_y^3, & Q_{12} = S_y^3 t_x^3 - C_y^3 t_z^3, \\ Q_{13} = C_y^2 t_z^2 - S_y^2 t_x^2, & Q_{14} = S_y^3 Q_9 + S_y^2 Q_{10}, \\ Q_{15} = S_y^2 Q_{12} + C_y^3 Q_9, & Q_{16} = S_y^3 Q_{13} + C_y^2 Q_{10}, \\ Q_{17} = C_y^2 Q_{12} + C_y^3 Q_{13}, & \end{cases}. \quad (10)$$

Considering a set of point correspondence  $\mathbf{x}^1 \leftrightarrow \mathbf{x}^2 \leftrightarrow \mathbf{x}^3$  from three views, its constraints can be expressed as:

$$[\mathbf{x}^2]_{\times} \left( \sum_i x_i^1 \mathbf{T}_i \right) [\mathbf{x}^3]_{\times} = \mathbf{0}_{3 \times 3}, \quad (11)$$

where  $\mathbf{x}^1 = [x_x^1, x_y^1, x_z^1]$ ,  $x_i^1$  denotes the  $i$ -th coordinate of  $\mathbf{x}^1$ . The corresponding image coordinates of view 2 and view 3 are denoted as  $\mathbf{x}^2$  and  $\mathbf{x}^3$ , and  $\mathbf{T}_i$  denotes the  $i$ -th matrix of the trifocal tensor.

Although Eq. (11) contains 9 equations, after analysis, we find that only 4 equations are independent. When there are 4 point correspondences, 16 independent equations can be constructed. Separating  $[Q_1 \ Q_2 \ \dots \ Q_{17}]^T$  from the

equations, the system of 16 equations can be expanded into matrix representations,

$$\begin{bmatrix} f_1^1 & f_2^1 & \dots & \dots & f_{17}^1 \\ f_1^2 & f_2^2 & \dots & \dots & f_{17}^2 \\ \dots & \dots & \dots & \dots & \dots \\ f_1^{16} & f_2^{16} & \dots & \dots & f_{17}^{16} \end{bmatrix} \begin{bmatrix} Q_1 \\ Q_2 \\ \dots \\ Q_{17} \end{bmatrix} = 0_{16 \times 1}. \quad (12)$$

The Eq. (12) is in the form of  $\mathbf{A}\mathbf{q} = 0$ , and  $\mathbf{q}$  is up to scale. Every element  $f_m^n$  in  $\mathbf{A}$  is known, where  $n$  represents the  $n$ -th independent equation, and  $m$  represents the coefficient of  $Q_m$ . By setting  $\|\mathbf{q}\| = 1$ , and using SVD decomposition, we can solve  $[Q_1 \ Q_2 \ \dots \ Q_{17}]^T$ . Then according to Eq. (10),  $\theta_2$ ,  $\mathbf{t}_2$ ,  $\theta_3$ ,  $\mathbf{t}_3$  can be calculated. The results can be further optimized using fixed constraints, and more details can be found in section III-D.

- Calculate  $\theta_2$ :

$$\begin{cases} S_y^2 = (Q_8 Q_9 + Q_{13} Q_{14}) / (Q_{10} Q_{13} - Q_9 Q_{12}) \\ C_y^2 = (Q_1 Q_{13} - Q_9 Q_{17}) / (Q_{10} Q_{13} - Q_9 Q_{12}) \\ \theta_2 = \arctan 2(S_y^2, C_y^2) \end{cases} \quad . \quad (13)$$

- Calculate  $\mathbf{t}_2$ :

$$\mathbf{t}_2 = \begin{bmatrix} C_y^2 Q_9 - S_y^2 Q_{13} \\ C_y^3 Q_4 - S_y^3 Q_5 \\ S_y^2 Q_9 + C_y^2 Q_{13} \end{bmatrix}. \quad (14)$$

- Calculate  $\theta_3$ :

$$\begin{cases} S_y^3 = -(Q_8 + S_y^2 Q_{12}) / Q_{13} \\ C_y^3 = (Q_1 - C_y^2 Q_{10}) / Q_9 \\ \theta_3 = \arctan 2(S_y^3, C_y^3) \end{cases} \quad . \quad (15)$$

- Calculate  $\mathbf{t}_3$ :

$$\mathbf{t}_3 = \begin{bmatrix} S_y^3 Q_{12} - C_y^3 Q_{10} \\ S_y^2 Q_7 - C_y^2 Q_2 \\ -S_y^3 Q_{10} - C_y^3 Q_{12} \end{bmatrix}. \quad (16)$$

After solving for  $\theta_2$ ,  $\mathbf{t}_2$ ,  $\theta_3$ ,  $\mathbf{t}_3$ , the relative pose estimation before vertical direction correction among the three views can be further recovered by using Eq. (5).

### C. The 3-point Case

Unlike Eq. (4),  $\mathbf{R}_k$  here takes the form of Cayley parameterization, and the form of  $\mathbf{t}_k$  remains unchanged.

$$\mathbf{R}_k = \frac{1}{1 + s_k^2} \begin{bmatrix} 1 - s_k^2 & 0 & 2s_k \\ 0 & 1 + s_k^2 & 0 \\ -2s_k & 0 & 1 - s_k^2 \end{bmatrix}, \mathbf{t}_k = \begin{bmatrix} t_x^k \\ t_y^k \\ t_z^k \end{bmatrix}, \quad (17)$$

where  $\theta_k$  represents the yaw angle,  $s_k = \tan(\theta_k/2)$ . In practice, the yaw angle is rarely equal to  $180^\circ$ , so this situation is almost negligible [23].

Substituting Eq. (17) into  $\mathbf{P}_k$ , and combining Eq. (2), then every equation in (11) can be expressed as :

$$\begin{aligned} & \frac{f_1^i(s_2, s_3)t_{2x} + f_2^i(s_2, s_3)t_{2y} + f_3^i(s_2, s_3)t_{2z}}{(1 + s_2^2)(1 + s_3^2)} \\ & + \frac{f_4^i(s_2, s_3)t_{3x} + f_5^i(s_2, s_3)t_{3y} + f_6^i(s_2, s_3)t_{3z}}{(1 + s_2^2)(1 + s_3^2)} = 0 \end{aligned}, \quad (18)$$

where  $f_*^i(s_2, s_3)$  is a polynomial with unknowns limited to  $s_2$  and  $s_3$ .  $i$  represents the  $i$ -th equation,  $i = 1, \dots, 9$ . Separating  $[t_{2x} \ t_{2y} \ t_{2z} \ t_{3x} \ t_{3y} \ t_{3z}]^T$  from (18), and define it as  $\mathbf{t}$ , the equations can be expanded into matrix representations.

$$\frac{1}{(1 + s_2^2)(1 + s_3^2)} \times \mathbf{F}(s_2, s_3)\mathbf{t} = \mathbf{0}_{6 \times 1}, \quad (19)$$

where

$$\mathbf{F}(s_2, s_3) = \begin{bmatrix} f_1^1 & f_2^1 & f_3^1 & f_4^1 & f_5^1 & f_6^1 \\ f_1^2 & f_2^2 & f_3^2 & f_4^2 & f_5^2 & f_6^2 \\ \dots & \dots & \dots & \dots & \dots & \dots \\ f_1^9 & f_2^9 & f_3^9 & f_4^9 & f_5^9 & f_6^9 \end{bmatrix}. \quad (20)$$

Although the dimensionality of  $\mathbf{F}(s_2, s_3)$  is  $9 \times 6$ , only 3 rows are independent. When there are 3 point correspondences, 27 equations can be constructed. By selecting independent rows of each point match, 9 equations can be constructed, and its matrix representations can be expressed as:

$$\widehat{\mathbf{F}}\mathbf{t} = \mathbf{0}_{6 \times 1}, \quad (21)$$

where

$$\widehat{\mathbf{F}} = \begin{bmatrix} f_1^1 & f_2^1 & f_3^1 & f_4^1 & f_5^1 & f_6^1 \\ f_1^2 & f_2^2 & f_3^2 & f_4^2 & f_5^2 & f_6^2 \\ f_1^4 & f_2^4 & f_3^4 & f_4^4 & f_5^4 & f_6^4 \\ f_1^{10} & f_2^{10} & f_3^{10} & f_4^{10} & f_5^{10} & f_6^{10} \\ f_1^{11} & f_2^{11} & f_3^{11} & f_4^{11} & f_5^{11} & f_6^{11} \\ f_1^{13} & f_2^{13} & f_3^{13} & f_4^{13} & f_5^{13} & f_6^{13} \\ f_1^{19} & f_2^{19} & f_3^{19} & f_4^{19} & f_5^{19} & f_6^{19} \\ f_1^{20} & f_2^{20} & f_3^{20} & f_4^{20} & f_5^{20} & f_6^{20} \\ f_1^{22} & f_2^{22} & f_3^{22} & f_4^{22} & f_5^{22} & f_6^{22} \end{bmatrix}. \quad (22)$$

The superscript of  $f_*^i$  is the  $i$ -th equation from 27 equations. According to the row sequences, every 3 rows are independent and correspond to a point match, such as rows 1, 2, and 4 corresponding to the first point match. Note that the multiple  $1/(1 + s_2^2)(1 + s_3^2)$  has been omitted in (21), but the multiple is still useful in the later paper. It can be used to reduce the degree of the polynomial in the determinant and enhance the solution efficiency.

Since there is a feasible solution  $\mathbf{t}$ , any 6 rows taken from  $\widehat{\mathbf{F}}$  can form a new matrix, and its determinant is 0,

$$F_1(s_2, s_3) = \begin{vmatrix} f_1^1 & f_2^1 & f_3^1 & f_4^1 & f_5^1 & f_6^1 \\ f_1^2 & f_2^2 & f_3^2 & f_4^2 & f_5^2 & f_6^2 \\ f_1^4 & f_2^4 & f_3^4 & f_4^4 & f_5^4 & f_6^4 \\ f_1^{10} & f_2^{10} & f_3^{10} & f_4^{10} & f_5^{10} & f_6^{10} \\ f_1^{11} & f_2^{11} & f_3^{11} & f_4^{11} & f_5^{11} & f_6^{11} \\ f_1^{13} & f_2^{13} & f_3^{13} & f_4^{13} & f_5^{13} & f_6^{13} \end{vmatrix}_{6 \times 6} = 0. \quad (23)$$

Then, we can obtain multiple equations similar to (23), which have 2 unknowns including  $s_2$ ,  $s_3$ . In the normal case, the equations can be solved, but it is not easy. Because (23) is of degree 24, solving high-degree equations is still a hard problem. Inspired by [31], we use the multiple  $1/(1 + s_2^2)(1 + s_3^2)$  to reduce the degree of the polynomial, the equations can be simplified as follows:

$$\text{quot} \left( \sum_{i=0}^{12} \sum_{j=0}^{12} w_{ij} s_2^i s_3^j, (1 + s_2^2)^3 (1 + s_3^2)^3 \right) = 0, \quad (24)$$

where  $\text{quot}(a, b)$  denotes the quotient of  $a$  divided by  $b$ . By simplifying, the degree of  $s_2$  and  $s_3$  is reduced to 6, and the total degree of the equations can be reduced to half of their original degree, i.e. the equations are of degree 12.

- Calculate  $s_2$  and  $s_3$ :

Using the latest Gröbner Automatic Solver proposed by [24], we can solve (24) accurately. Even though Eq. (24) has been simplified, the equation degree is still very high. As a result, the solution process is time-consuming. The Solver would obtain 6 complex roots, from which we choose all the real roots as possible solutions for  $s_2$  and  $s_3$ .

- Calculate  $\mathbf{t}$ :

After  $s_2$  and  $s_3$  are solved, we substitute  $s_2$  and  $s_3$  into  $\hat{\mathbf{F}}$  in (21). By setting  $|\mathbf{t}| = 1$ , and using SVD decomposition, we can solve  $[t_{2x} \ t_{2y} \ t_{2z} \ t_{3x} \ t_{3y} \ t_{3z}]^T$ .

#### D. Constraint Enforcement

No matter the 4-point case or the 3-point case, we can both get the trifocal tensor  $\mathbf{T}_i$ , but it does not strictly satisfy the constraints of Eq. (2), so it is necessary to enforce constraints on  $\mathbf{T}_i$  to improve its accuracy further.

Assuming  $u_i$  and  $v_i$  are the left and right null-vectors of  $\mathbf{T}_i$  respectively, i.e.  $\mathbf{u}_i^\top \mathbf{T}_i = \mathbf{0}^\top$ ,  $\mathbf{T}_i \mathbf{v}_i = \mathbf{0}$ , the epipoles  $\mathbf{e}'$  and  $\mathbf{e}''$  are perpendicular to the three left and right null-vectors of  $\mathbf{T}_i$ . Using SVD decomposition, the epipoles can be obtained.

$$\begin{cases} \mathbf{e}'^\top [\mathbf{u}_1, \mathbf{u}_2, \mathbf{u}_3] = \mathbf{0} \\ \mathbf{e}''^\top [\mathbf{v}_1, \mathbf{v}_2, \mathbf{v}_3] = \mathbf{0} \end{cases} \quad (25)$$

According to Eq. (6) and the obtained epipoles, the projection matrices  $P_2$  and  $P_3$  can be expressed as follows:

$$\mathbf{P}_2 = \begin{bmatrix} a_1 & 0 & a_2 & e'_1 \\ 0 & a_3 & 0 & e'_2 \\ -a_2 & 0 & a_1 & e'_3 \end{bmatrix}, \quad (26)$$

$$\mathbf{P}_3 = \begin{bmatrix} a_4 & 0 & a_5 & e''_1 \\ 0 & a_6 & 0 & e''_2 \\ -a_5 & 0 & a_4 & e''_3 \end{bmatrix}, \quad (27)$$

where  $a_*$  represents the unknowns,  $e'_i$  or  $e''_i$  is the  $i$ -th element of epipoles. Then using Eq. (2), we can get the trifocal tensor  $\mathbf{T}_i$ .

$$\mathbf{T}_1 = \begin{bmatrix} -a_4e'_1 + a_1e''_1 & a_1e''_2 & a_5e'_1 + a_1e''_3 \\ -a_4e'_2 & 0 & a_5e'_2 \\ -a_4e'_3 - a_2e'_1 & -a_2e''_2 & a_5e'_3 - a_2e''_3 \end{bmatrix}, \quad (28)$$

$$\mathbf{T}_2 = \begin{bmatrix} 0 & -a_6e'_1 & 0 \\ a_3e''_1 & -a_6e'_2 + a_3e''_2 & a_3e''_3 \\ 0 & -a_6e'_3 & 0 \end{bmatrix}, \quad (29)$$

$$\mathbf{T}_3 = \begin{bmatrix} -a_5e'_1 + a_2e''_1 & a_2e''_2 & -a_4e'_1 + a_2e''_3 \\ -a_5e'_2 & 0 & -a_4e'_2 \\ -a_5e'_3 + a_1e''_1 & a_1e''_2 & -a_4e'_3 + a_1e''_3 \end{bmatrix}. \quad (30)$$

Comparing Eq. (28) to (30) with Eq. (7) to (9), we can find that  $Q_*$  in Eq. (7) to Eq. (9) can be expressed as expressions of unknowns  $a_*$ , its linear relationships can be expressed as:

$$\mathbf{q} = \mathbf{E}\mathbf{a}. \quad (31)$$

The main advantage of Eq. (28) to (30) is that they naturally satisfy the constraint in Eq. (2). Then the problem in Eq. (12), i.e.  $\mathbf{A}\mathbf{q} = \mathbf{0}$  can be transformed into the following form:

$$\mathbf{a} = \arg \min_{\mathbf{a}} (\|\mathbf{A}\mathbf{E}\mathbf{a}\|) \text{ s.t. } \|\mathbf{E}\mathbf{a}\| = 1 \quad (32)$$

After  $\mathbf{a}$  is solved, then using Eq. (28) to (30) solve the trifocal tensor  $\mathbf{T}_i$ , and its results are more accurate. All the above content outlines our entire process, other methods [27] [28] may also be viable and require further exploration.

## IV. EXPERIMENTS

In order to validate the accuracy and feasibility of our method, both synthetic and real-world experiments are independently conducted in the paper. Since most 3-view problem solvers do not have open source code, or some have code but no comparison, we have not found an effective way to compare our method with the latest solver [6] yet. So, except for the public 3-view normalized linear solution [10], we also compare our method with some classic mature 2-view algorithms, including 8pt-Hartley-2view [10], and 5pt-Nister-2view [9] methods, which can also be used for the 3-view pose estimation. Different from the method [6], which requires GPU implementations, the above methods are all based on CPU implementations. In this paper, our proposed methods are referred to as 3pt-Our-3view and 4pt-Our-3view, the ordinary normalized solution for the 3-view problem is referred to as 7pt-Hartley-3view, and its code can be found in [7]. Since 2-view and 3-view are different and each has its own advantages, our experiments are not intended to prove that our methods outperform 2-view algorithms, but to illustrate the feasibility and practicality of the proposed methods.

In the experiment, the rotation and translation errors are calculated as follows:

$$\varepsilon_{\mathbf{R}} = \arccos((\text{trace}(\mathbf{R}_{gt}\mathbf{R}^T) - 1)/2), \quad (33)$$

$$\varepsilon_{\mathbf{t}} = \arccos((\mathbf{t}_{gt}^T \mathbf{t})/(\|\mathbf{t}_{gt}\| \cdot \|\mathbf{t}\|)), \quad (34)$$

where  $\mathbf{R}_{gt}$  and  $\mathbf{t}_{gt}$  are the ground truth values,  $\mathbf{R}$  and  $\mathbf{t}$  are the estimated values. Since the estimated translation of the monocular camera is up to scale, we adopt the angle metric to measure the translation errors instead of using Euclidean distance. After  $\varepsilon_{\mathbf{R}}$  and  $\varepsilon_{\mathbf{t}}$  among three views are solved, we choose the median values as the final results.

#### A. Efficiency Comparison and Numerical Stability

All methods run on the same computer, i.e. Intel(R) Xeon(R) Gold6133 2.50GHz using MATLAB. The detailed run times are shown in Table I, we can see that the proposed 4pt-Our-3view method has a runtime of 0.95 ms, which is longer than the 0.63 ms of the 8pt-Hartley-2view method, but it can solve two sets of camera poses at the same time, while the 8-point method only solves one set, so it is more efficient than the 8pt-Hartley-2view method. The 4pt-Our-3view method runs 4 times faster than the 7pt-Hartley-3view method and is the most efficient algorithm in the 3-view problem. The 3pt-Our-3view

method adopts the Gröbner-based approach, and its polynomial coefficients are quite complex. However, it can still operate in real-time and runs 1.4 times faster than the 7pt-Hartley-3view method.

TABLE I  
RUN-TIME COMPARISON OF DIFFERENT METHODS(UNIT:MS)

Methods	8pt-Hartley-2view	5pt-Nister-2view	7pt-Hartley-3view	3pt-Our-3view	4pt-Our-3view
Time	0.63	1.46	4.24	2.93	0.95

Numerical stability refers to the ability of an algorithm to provide consistent, accurate, and reliable pose estimation under ideal or perfect conditions. Without considering the influence of image noises, the detailed results regarding numerical stability are shown in Fig. 3. All the methods are executed 5,000 times. The results show that the 4pt-Our-3view method is the most stable, followed by the 5pt-Nister-2view and 8pt-Hartley-2view methods. Although the proposed 3pt-Our-3view method has the worst stability, its mean error is less than  $1e-13$ , and most errors are less than  $1e-8$ , so the 3pt-Our-3view method is still accurate and feasible.

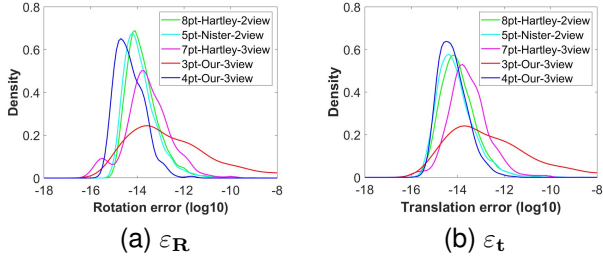


Fig. 3. Probability density functions over relative pose estimation errors. (a) Rotation estimation errors. (b) Translation estimation errors. The horizontal axis represents the  $\log_{10}$  value of the estimated error, and the vertical axis represents the probability density. The narrower the curve, the smaller the data variance, indicating that the algorithm is more stable

### B. Experiments on Synthetic Data

In the synthetic experiments, the image resolution is  $640 \times 480$  pixels, and its principal point is  $(320, 240)$ . The rotation angles among the three views are set within a range of  $-10^\circ$  to  $10^\circ$ , and the distances between each other are set within a range of  $-10$  m to  $10$  m. 3D points in space are randomly generated and can be observed by three views simultaneously. In the simulation, the effects of image noise and IMU angle noise on each method were studied separately. All the methods were executed 1000 times.

1) *Accuracy with image noise*: To study the effects of image noise on the algorithm, in the simulation, we applied Gaussian noise varying from 0 to 2 pixels. The results in Fig. 4 show that the 3pt-Our-3view method performs best when solving rotation matrices, followed by 4pt-Our-3view and 5pt-Nister-2view methods. As for solving translation vectors, the 5pt-Nister-2view method demonstrates the highest level of accuracy. Despite this, the accuracy of the 3pt-Our-3view method also performs well with accuracy almost close to the 5pt-Nister-2view method, and has the advantage of solving more parameters with fewer point

correspondences. The 7pt-Hartley-3view method performs worst and is susceptible to image noise. As for the 3-view problem, compared with 7pt-Hartley-3view, the advantages of 3pt-Our-3view and 4pt-Our-3view are obvious.

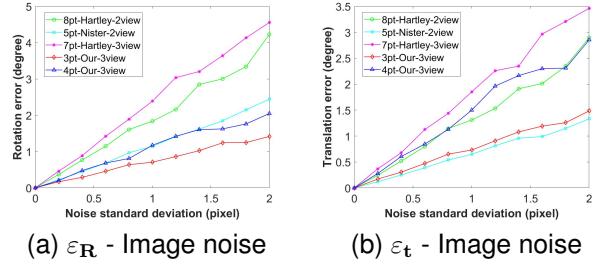


Fig. 4. Methods accuracy with image noise. (a) Rotation estimation errors. (b) Translation estimation errors.

2) *Accuracy with IMU pitch angle noise*: In most cases, a low-cost IMU has an angle accuracy of  $0.5^\circ$ , while that of a high-performance IMU is only  $0.02^\circ$  [32]. In practical applications, the accuracy of the IMUs used in cars or modern smartphones is approximately  $0.06^\circ$  [33]. To study the effects of IMU angle noise on the algorithm, in the simulation, we set the IMU angle noise ranging from  $0^\circ$  to  $1^\circ$ . The image noise was kept constant at 1 pixel. Since the 8pt-Hartley-2view, 5pt-Nister-2view and 7pt-Hartley-3view methods don't use IMUs measurement information, these methods are not affected by the IMU angle noise, so we take the mean values as the final results in Fig. 5. Although

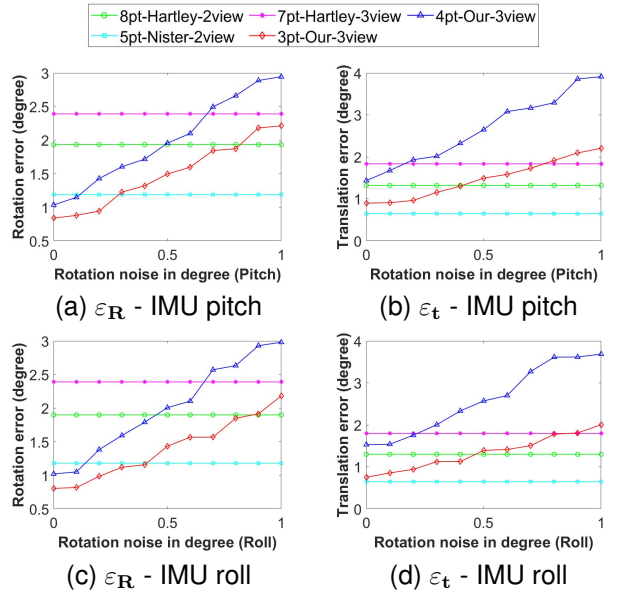


Fig. 5. Methods accuracy with IMU angle noise. (a) Rotation estimation errors with IMU pitch angel noise. (b) Translation estimation errors with IMU pitch angel noise. (c) Rotation estimation errors with IMU roll angel noise. (d) Translation estimation errors with IMU roll angel noise.

the 4pt-Our-3view and 3pt-Our-3view methods are affected by IMU angle noise, the rotation accuracy is still superior to the 7pt-Hartley-3view method, or even better than the 8pt-Hartley-2view method when the inertial navigation error is less than  $0.5^\circ$ . The translation accuracy is more susceptible to the influence of inertial navigation

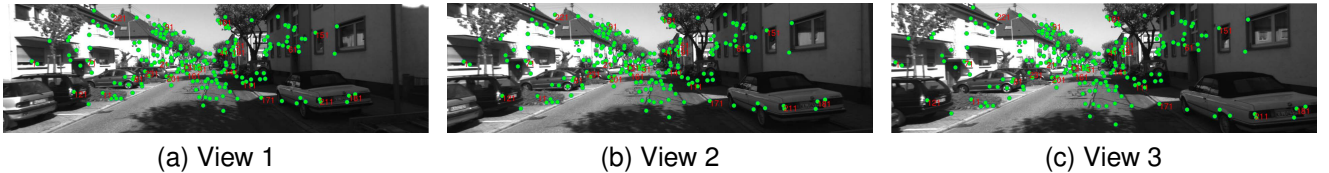


Fig. 6. Point correspondences of triple images. The pictures were taken from sequential images 56 to 58 in sequence 00 of the KITTI dataset.

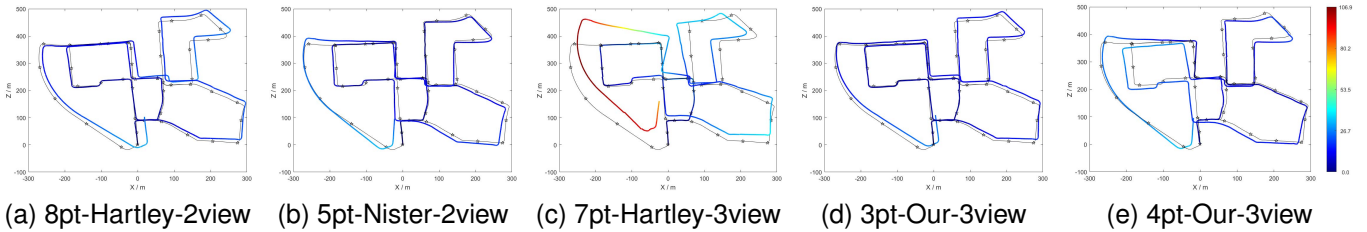


Fig. 7. Estimated visual odometry trajectories for KITTI sequences 00 (unit: meter). (a) Trajectory estimation with 8pt-Hartley-2view method, (b) Trajectory estimation with 5pt-Nister-2view method, (c) Trajectory estimation with 7pt-Hartley-3view method, (d) Trajectory estimation with 3pt-Our-3view method, (e) Trajectory estimation with 4pt-Our-3view method.

angle noise, but they are still within a reasonable range, and the 3pt-Our-3view method is still superior to the 7pt-Hartley-3view or 8pt-Hartley-2view method.

### C. Experiments on Real-world Data

The real-world performances of the proposed method were evaluated on the KITTI benchmarks, currently the largest dataset for evaluating computer vision algorithms in autonomous driving scenarios. The KITTI dataset has many sequences, from which sequences 00-10 can provide ground truth values measured by the built-in GPS/IMU units. To evaluate the efficacy of the proposed method in the real world, we compared its performance on all eleven sequences.

All methods adopt the SIFT algorithm [34] to extract the point correspondences of triple images. From Fig. 6, we can see that there are three consecutive images, and 376 point correspondences (indicated by green dots) can be obtained, and their corresponding relationships are indicated by red numbers. For the sake of visibility, only a few of the red numbers are indicated in the figure.

To eliminate the influence of outliers, all methods are integrated with the RANSAC framework. As for RANSAC parameters, distances are calculated using the Sampson error, and all methods use the same distance threshold. It should be noted that all final pose results are the initial solutions with the largest number of inlier points, that is, the results are not optimized by subsequent optimization algorithms. The median errors for rotation estimation and translation estimation are utilized to assess the performance of each method, its detailed results can be seen in Table II and Table III.

1) *Rotation errors*: From Table II, we can see that the 3pt-Our-3view method has the smallest rotational errors in the KITTI dataset, followed by the 4pt-Our-3view method, which is also consistent with the results of synthetic experiments. The 7pt-Hartley-3view and 8pt-Hartley-2view methods have the worst rotation accuracy. Overall, the performance of the 3pt-Our-3view

TABLE II  
MEDIAN ROTATION ERRORS FOR KITTI SEQUENCES(UNIT: DEGREE)

Seq.	8pt-Hartley-2view	5pt-Nister-2view	7pt-Hartley-3view	3pt-Our-3view	4pt-Our-3view
00	0.160	0.086	0.118	<b>0.042</b>	0.043
01	0.502	0.080	0.450	<b>0.047</b>	0.055
02	0.157	0.086	0.123	<b>0.042</b>	<b>0.042</b>
03	0.163	0.076	0.134	<b>0.050</b>	<b>0.050</b>
04	0.172	0.074	0.135	<b>0.028</b>	0.036
05	0.151	0.066	0.103	0.032	<b>0.031</b>
06	0.150	0.065	0.116	<b>0.031</b>	0.034
07	0.135	0.069	0.107	<b>0.033</b>	0.034
08	0.146	0.075	0.109	<b>0.032</b>	0.034
09	0.164	0.082	0.130	<b>0.038</b>	0.039
10	0.154	0.081	0.120	<b>0.034</b>	<b>0.034</b>

and 4pt-Our-3view methods is 2-3 times more accurate than other methods.

2) *Translation errors*: Compared with the rotation errors, the translation errors of each method are bigger. The translation errors have more outliers, which has a certain impact on the accuracy of all the methods. From Table III, we can see that the 5pt-Nister-2view method performs best. Similar to the synthetic experiments, the accuracy of the 3pt-Our-3view method performs almost close to the 5pt-Nister-2view, and even higher in sequences 04, 06, and 07.

TABLE III  
MEDIAN TRANSLATION ERRORS FOR KITTI SEQUENCES(UNIT: DEGREE)

Seq.	8pt-Hartley-2view	5pt-Nister-2view	7pt-Hartley-3view	3pt-Our-3view	4pt-Our-3view
00	1.498	<b>1.178</b>	1.296	1.296	1.436
01	3.148	<b>2.095</b>	3.874	2.435	3.53
02	1.411	<b>1.124</b>	1.240	1.238	1.381
03	1.780	<b>1.306</b>	1.663	1.587	1.863
04	1.286	1.076	1.059	<b>0.789</b>	1.221
05	1.294	<b>0.970</b>	1.077	1.030	1.217
06	1.040	0.812	0.900	<b>0.782</b>	0.985
07	1.692	1.300	1.490	<b>1.267</b>	1.562
08	1.653	<b>1.368</b>	1.499	1.429	1.625
09	1.393	<b>1.008</b>	1.217	1.034	1.237
10	1.609	<b>1.058</b>	1.336	1.256	1.367

To visualize the comparison of all methods, we also plotted the camera's trajectory in Fig. 7. Since the estimated transla-

tion of the monocular camera is up to scale, all the methods use the ground truth scale to recover its real translation. In Fig. 7, the black trajectory represents the ground truth, the colored trajectory represents the estimated values, and its color encodes the magnitude of the absolute trajectory error (ATE) [35]. Because of space constraints, only the trajectory of sequence 00 is presented. As can be seen from Fig. 7, compared with the 7pt-Hartley-3view method, the 3pt-Our-3view and 4pt-Our-3view methods have smaller ATE, which also indirectly illustrates the accuracy of our proposed methods.

## V. CONCLUSION

In this paper, we derived the methods based on 4 or 3 point correspondences to solve the 3-view problem with IMU measurement data. First, by using the angle information measured by IMUs, the 3-view problem can be effectively simplified. Then, by utilizing either 4 point correspondences or 3 point correspondences, we can derive the linear closure solution and the minimal solution, respectively. Experiments on synthetic data and real-world data show that our methods are accurate and feasible. In the application of autonomous driving or drone navigation, our algorithm can provide an effective backup option when 2-view methods fail.

## REFERENCES

- [1] B. Li, L. Heng, G. H. Lee, and M. Pollefeys, “A 4-point algorithm for relative pose estimation of a calibrated camera with a known relative rotation angle,” in *IEEE/RSJ International Conference on Intelligent Robots and Systems*, 2013, pp. 1595–1601.
- [2] C. Campos, R. Elvira, J. J. G. Rodríguez, J. M. Montiel, and J. D. Tardós, “Orb-slam3: An accurate open-source library for visual, visual-inertial, and multimap slam,” *IEEE Transactions on Robotics*, vol. 37, no. 6, pp. 1874–1890, 2021.
- [3] R. Mur-Artal and J. D. Tardós, “Orb-slam2: An open-source slam system for monocular, stereo, and rgb-d cameras,” *IEEE Transactions on Robotics*, vol. 33, no. 5, pp. 1255–1262, 2017.
- [4] Z. Yu, B. Guan, S. Liang, Z. Li, S. Ye, and Q. Yu, “Globally optimal relative pose estimation using affine correspondences with known vertical direction,” *IEEE Transactions on Instrumentation and Measurement*, vol. 72, pp. 1–12, 2023.
- [5] D. Nistér and F. Schaffalitzky, “Four points in two or three calibrated views: Theory and practice,” *International Journal of Computer Vision*, vol. 67, pp. 211–231, 2006.
- [6] Y. Ding, C.-H. Chien, V. Larsson, K. Åström, and B. Kimia, “Minimal solutions to generalized three-view relative pose problem,” in *IEEE International Conference on Computer Vision*, 2023, pp. 8156–8164.
- [7] L. F. Julià and P. Monasse, “A critical review of the trifocal tensor estimation,” in *Pacific-Rim Symposium on Image and Video Technology*, 2018, pp. 337–349.
- [8] M. A. Fischler and R. C. Bolles, “Random sample consensus: a paradigm for model fitting with applications to image analysis and automated cartography,” *Communications of the ACM*, vol. 24, no. 6, pp. 381–395, 1981.
- [9] D. Nistér, “An efficient solution to the five-point relative pose problem,” *Transactions on Pattern Analysis and Machine Intelligence*, vol. 26, no. 6, pp. 756–770, 2004.
- [10] R. Hartley and A. Zisserman, *Multiple view geometry in computer vision*. Cambridge university press, 2003.
- [11] R. J. Holt and A. N. Netravali, “Motion and structure from line correspondences: Some further results,” *International Journal of Imaging Systems and Technology*, vol. 5, no. 1, pp. 52–61, 1994.
- [12] R. Fabbri, T. Duff, H. Fan, M. H. Regan, D. d. C. d. Pinho, E. Tsigaridas, C. W. Wampler, J. D. Hauenstein, P. J. Giblin, B. Kimia, et al., “Trplp-trifocal relative pose from lines at points,” in *IEEE Conference on Computer Vision and Pattern Recognition*, 2020, pp. 12 073–12 083.
- [13] B. Guan, P. Vasseur, and C. Demonceaux, “Trifocal tensor and relative pose estimation from 8 lines and known vertical direction,” in *IEEE/RSJ International Conference on Intelligent Robots and Systems*, 2022, pp. 6001–6008.
- [14] A. Heyden, “Reconstruction from image sequences by means of relative depths,” *International Journal of Computer Vision*, vol. 24, no. 2, pp. 155–161, 1997.
- [15] C. Ressl, “A minimal set of constraints and a minimal parameterization for the trifocal tensor,” *International Archives of Photogrammetry Remote Sensing and Spatial Information Sciences*, vol. 34, no. 3/A, pp. 277–282, 2002.
- [16] K. Nordberg, “A minimal parameterization of the trifocal tensor,” in *IEEE Conference on Computer Vision and Pattern Recognition*, 2009, pp. 1224–1230.
- [17] O. Faugeras and T. Papadopoulo, “A nonlinear method for estimating the projective geometry of 3 views,” in *IEEE International Conference on Computer Vision*, 1998, pp. 477–484.
- [18] J. Ponce and M. Hebert, “Trinocular geometry revisited,” in *IEEE Conference on Computer Vision and Pattern Recognition*, 2014, pp. 17–24.
- [19] P. Hruba, T. Duff, A. Leykin, and T. Pajdla, “Learning to solve hard minimal problems,” in *IEEE Conference on Computer Vision and Pattern Recognition*, 2022, pp. 5532–5542.
- [20] Z. Xu, Y. He, H. Wei, B. Xu, B. Xie, and Y. Wu, “An accurate and real-time relative pose estimation from triple point-line images by decoupling rotation and translation,” *arXiv preprint arXiv:2403.11639*, 2024.
- [21] Z. Kukelova, M. Bujnak, and T. Pajdla, “Automatic generator of minimal problem solvers,” in *European Conference on Computer Vision*, 2008, pp. 302–315.
- [22] V. Larsson, M. Oskarsson, K. Astrom, A. Wallis, Z. Kukelova, and T. Pajdla, “Beyond grobner bases: Basis selection for minimal solvers,” in *IEEE Conference on Computer Vision and Pattern Recognition*, 2018, pp. 3945–3954.
- [23] V. Larsson, K. Astrom, and M. Oskarsson, “Efficient solvers for minimal problems by syzygy-based reduction,” in *IEEE Conference on Computer Vision and Pattern Recognition*, 2017, pp. 820–829.
- [24] B. Li and V. Larsson, “Gaps: Generator for automatic polynomial solvers,” *arXiv preprint arXiv:2004.11765*, 2020.
- [25] S. Bhayani, Z. Kukelova, and J. Heikkilä, “A sparse resultant based method for efficient minimal solvers,” in *IEEE Conference on Computer Vision and Pattern Recognition*, 2020, pp. 1770–1779.
- [26] E. Martyushev, S. Bhayani, and T. Pajdla, “Automatic solver generator for systems of laurent polynomial equations,” *arXiv preprint arXiv:2307.00320*, 2023.
- [27] Z. Kukelova, J. Kileel, B. Sturmfels, and T. Pajdla, “A clever elimination strategy for efficient minimal solvers,” in *IEEE Conference on Computer Vision and Pattern Recognition*, 2017, pp. 4912–4921.
- [28] Y. Ding, Y. Su, C. Xu, J. Yang, and H. Kong, “A general elimination strategy for camera motion estimation,” in *2021 IEEE International Conference on Robotics and Automation*. IEEE, 2021, pp. 9333–9339.
- [29] A. J. Sommese, C. W. Wampler, et al., *The Numerical solution of systems of polynomials arising in engineering and science*. World Scientific, 2005.
- [30] C.-H. Chien, H. Fan, A. Abdelfattah, E. Tsigaridas, S. Tomov, and B. Kimia, “Gpu-based homotopy continuation for minimal problems in computer vision,” in *IEEE Conference on Computer Vision and Pattern Recognition*, 2022, pp. 15 765–15 776.
- [31] B. Guan, J. Zhao, D. Barath, and F. Fraundorfer, “Minimal solvers for relative pose estimation of multi-camera systems using affine correspondences,” *International Journal of Computer Vision*, vol. 131, no. 1, pp. 324–345, 2023.
- [32] Z. Kukelova, M. Bujnak, and T. Pajdla, “Closed-form solutions to minimal absolute pose problems with known vertical direction,” in *Asian Conference on Computer Vision*, 2010, pp. 216–229.
- [33] Y. Ding, D. Barath, J. Yang, H. Kong, and Z. Kukelova, “Globally optimal relative pose estimation with gravity prior,” in *IEEE Conference on Computer Vision and Pattern Recognition*, 2021, pp. 394–403.
- [34] D. G. Lowe, “Distinctive image features from scale-invariant keypoints,” *International journal of computer vision*, vol. 60, pp. 91–110, 2004.
- [35] J. Sturm, N. Engelhard, F. Endres, W. Burgard, and D. Cremers, “A benchmark for the evaluation of rgb-d slam systems,” in *IEEE/RSJ International Conference on Intelligent Robots and Systems*, 2012, pp. 573–580.